J. Phys.: Condens. Matter **24** (2012) 435403 (9pp) doi:10.1088/0953-8984/24/43/435403

Structural properties of $PbVO_3$ perovskites under hydrostatic pressure conditions up to 10.6 GPa

Wei Zhou[1,2], Dayong Tan[1], Wansheng Xiao[1], Maoshuang Song[2], Ming Chen[1,2], Xiaolin Xiong[2] and Jian Xu[3,4]

[1] Key Laboratory of Mineralogy and Metallogeny, Guangzhou Institute of Geochemistry, Chinese Academy of Sciences, Guangzhou 510640, People's Republic of China
[2] State Key Laboratory of Isotope Geochemistry, Guangzhou Institute of Geochemistry, Chinese Academy of Sciences, Guangzhou 510640, People's Republic of China
[3] Institute of Atomic and Molecular Physics, Sichuan University, Chengdu, 610065, People's Republic of China
[4] Institute of Fluid Physics, China Academy of Engineering Physics, Mianyang, 621900, People's Republic of China

E-mail: wsxiao@gig.ac.cn and msong@gig.ac.cn

Received 7 July 2012, in final form 9 September 2012
Published 8 October 2012
Online at stacks.iop.org/JPhysCM/24/435403

Abstract
High-pressure synchrotron x-ray powder diffraction experiments were performed on $PbVO_3$ tetragonal perovskite in a diamond anvil cell under hydrostatic pressures of up to 10.6 GPa at room temperature. The compression behavior of the $PbVO_3$ tetragonal phase is highly anisotropic, with the *c*-axis being the soft direction. A reversible tetragonal to cubic perovskite structural phase transition was observed between 2.7 and 6.4 GPa in compression and below 2.2 GPa in decompression. This transition was accompanied by a large volume collapse of 10.6% at 2.7 GPa, which was mainly due to electronic structural changes of the V^{4+} ion. The polar pyramidal coordination of the V^{4+} ion in the tetragonal phase changed to an isotropic octahedral coordination in the cubic phase. Fitting the observed *P–V* data using the Birch–Murnaghan equation of state with a fixed K_0' of 4 yielded a bulk modulus $K_0 = 61(2)$ GPa and a volume $V_0 = 67.4(1)$ Å^3 for the tetragonal phase, and the values of $K_0 = 155(3)$ GPa and $V_0 = 58.67(4)$ Å^3 for the cubic phase. The first-principles calculated results were in good agreement with our experiments.

(Some figures may appear in colour only in the online journal)

1. Introduction

Multiferroic materials, in which ferromagnetism and ferroelectricity coexist, have stimulated a great deal of experimental and theoretical interest in recent years due to their considerable technological and fundamental importance [1–5]. The $PbVO_3$ tetragonal perovskite (*P*4*mm*) (*T*-phase) was synthesized recently at high pressures and suggested to be a candidate multiferroic with a two-dimensional C-type antiferromagnetism (C-AFM) ordering and a large ferroelectric polarization [6–8]. The $PbVO_3$ *T*-phase is isostructural with $PbTiO_3$, but exhibits a more pronounced structural distortion and a much larger unit cell volume. The V^{4+} ion in the *T*-phase deviates markedly from the center of the VO_6 octahedron in the ideal perovskite structure, leading to a much longer V–O1 bond and a very short V–O1 bond along the *c*-axis. Thus, the $PbVO_3$ *T*-phase presents a VO_5 pyramidal rather than a VO_6 octahedral coordination as shown in figure 1(a). The large distortion manifests as a high c/a ratio of 1.229 and a calculated spontaneous polarization of 152 μC cm^{-2} [9]. It has been suggested that both the tendency of the V^{4+} ion to form a short vanadyl bond and the stereo effect of the $6s^2$ electronic lone pair of the Pb^{2+} ion play crucial roles in the large tetragonal distortion of $PbVO_3$ [6,

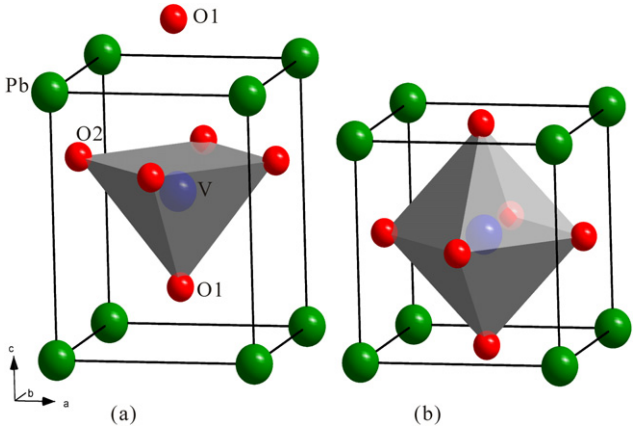

Figure 1. Crystal structures of $PbVO_3$ perovskites. (a) The tetragonal phase (T-phase, $P4mm$), five O atoms (or O^{2-} ions) are coordinated with a central V atom (or V^{4+} ion), forming a VO_5 square pyramid. Base vertex O atoms are denoted as O2 and the apex O atom is denoted as O1. (b) The cubic phase (C-phase, $Pm\bar{3}m$), six O atoms coordinated with a central V atom are arranged in a VO_6 octahedral configuration.

10]. As a result, the $PbVO_3$ T-phase is stable over a wide range of temperatures, up to its oxidation temperature of 570 K [7].

ABO_3-type ferroelectric (FE) compounds with perovskite structures often transform to a paraelectric (PE) phase when the temperature or pressure changes [11–13]. For instance, the $PbTiO_3$ tetragonal perovskite ($P4mm$) transforms to cubic perovskite ($Pm\bar{3}m$) at a high temperature of 763 K or at a high pressure of 11.2 GPa [14, 15]. $BaTiO_3$ perovskite also exhibits a tetragonal ($P4mm$) to cubic ($Pm\bar{3}m$) phase transition at a high pressure of about 2 GPa or a high temperature of 393 K [16]. The polymorphic transitions in the perovskite structural compounds often lead to a minor volume discontinuity [15, 17] so that the transitions are considered as near second-order phase transitions. However, significant volume collapse has also been observed in some compounds such as $BiCoO_3$ perovskite and orthoferrites ($RFeO_3$, R = Pr, Eu, Lu), indicating first-order transitions related to modification of electronic structure [18]. The $BiCoO_3$ perovskite, which is isotypic with $PbVO_3$ at ambient conditions, was reported to exhibit a tetragonal ($P4mm$) to orthorhombic ($Pnma$) transition at 3–4 GPa accompanying a volume collapse as large as 13% [18]. This is the largest volume change induced by a perovskite polymorphic phase transition reported to date. The tetragonality of the $PbVO_3$ tetragonal perovskite ($c/a = 1.23$) is similar to that of $BiCoO_3$ ($c/a = 1.27$) but is much larger than that of $PbTiO_3$ ($c/a = 1.06$) and $BaTiO_3$ ($c/a = 1.01$). The abnormally large tetragonality of the perovskite compounds, which indicates a large distortion and a large lattice volume, implies a structural instability and the possible existence of a first-order polymorphic phase transition, with a clear volume change at high pressures or high temperatures. However, the possible transition of the polar $PbVO_3$ T-phase to a paraelectric phase has not been observed up to the oxidation temperature of 570 K at atmospheric pressure. Therefore, high-pressure experiments can provides a means of revealing the nature of a possible phase transition for the $PbVO_3$ T-phase.

Synchrotron energy dispersive x-ray diffraction (EDXRD) experiments have been carried out on the $PbVO_3$ T-phase at high pressures up to 5.9 GPa using a cubic anvil-type apparatus [7]. The obtained x-ray diffraction patterns indicate that a reversible but sluggish first-order phase transition from the tetragonal phase to a new phase possibly with a cubic perovskite structure starts at about 2 GPa and room temperature. This phase transition is characterized by a volume collapse of 12.3%, phase coexistence over a large pressure range, and a large hysteresis. However, the limited resolution of the EDXRD patterns and the limited number of observed diffraction lines of the possible cubic phase do not facilitate an understanding of the high pressure behaviors of both the $PbVO_3$ tetragonal and cubic perovskites and the details of the phase transition between them [7]. First-principles calculations were also performed to investigate the pressure-induced phase transition of the $PbVO_3$ perovskites [19]. A total energy calculation using the GGA exchange and correlated function in the WC scheme predicted a C-AFM insulator for the $PbVO_3$ T-phase, correctly describing the experimental results. The $PbVO_3$ T-phase collapsed to a nonmagnetic metal with a cubic perovskite structure as the pressure was increased to 1.75 GPa. The phase transition led to a large volume change of 10.6%. However, detailed information about the high-pressure behaviors of the two types of $PbVO_3$ perovskites, such as the atomic fractional coordinates and the parameters for the equation of states (EOS), have not been presented in the theoretical study yet.

To understand the structural features of the $PbVO_3$ T-phase at high pressures and to clarify the nature of the possible cubic perovskite high-pressure polymorph of $PbVO_3$, we have carried out *in situ* high-pressure experiments with a diamond anvil cell (DAC) apparatus combined with a synchrotron angle dispersive x-ray diffraction (ADXRD) technique under hydrostatic pressure conditions. We also performed first-principles calculations on the high-pressure behavior of the $PbVO_3$ perovskites in order to describe and complement the experimental results.

2. Experimental and theoretical methods

2.1. Experimental details

The $PbVO_3$ perovskite sample used in this study was synthesized in a symmetric Mao-Bell-type DAC by decomposing the $Pb_2V_2O_7$ compound under high pressure and high temperature conditions. The raw material, $Pb_2V_2O_7$, was prepared by heating stoichiometric amounts of PbO and V_2O_5 in a platinum crucible in an electric furnace. We first ground the mixture of PbO and V_2O_5 and then melted it at 800 °C and kept it at this temperature for 2 h. Then the mixture was cooled to 700 °C and kept at this temperature for 3 h before being quenched to room temperature. The x-ray diffraction pattern of the crystallized raw $Pb_2V_2O_7$ sample can be indexed as a monoclinic structure with lattice parameters

of $a = 13.328(1)$ Å, $b = 7.1476(5)$ Å, $c = 7.097(1)$ Å, $\beta = 105.97(1)°$, and $V = 650.0(1)$ Å^3. The values for these parameters are in good agreement with the single-crystal x-ray diffraction results for monoclinic $Pb_2V_2O_7$ (space group $P2_1/a$, $Z = 4$) [20].

The $PbVO_3$ perovskite sample was synthesized by the DAC laser-heating technique. First a gasket was prepared by indenting a piece of T301 stainless steel foil to a thickness of approximately 40 μm and then drilling a 120 μm hole, which served as the sample chamber, near the center of the indented area. The $Pb_2V_2O_7$ sample was pressed into a pellet with a thickness of approximately 15 μm and a piece of sample approximately 60 μm in diameter was loaded into the sample chamber. Argon, which was used as a pressure-transmitting medium and the thermal-insulating medium during laser heating here, was cryogenically loaded into the sample chamber. A few fine ruby chips were loaded into the chamber to enable *in situ* sample pressure measurements by standard ruby fluorescence spectroscopy [21]. The sample in the DAC was pressurized up to approximately 30 GPa and heated with a YAG laser to temperatures of approximately 1500–2000 K before being released to ambient pressure. Examination of the released sample revealed that it was the $PbVO_3$ *T*-phase with minor impurities (as shown in figure 2(a)). This result indicates that the $Pb_2V_2O_7$ compound has reacted to form a $PbVO_3$ perovskite with the valence of the V ion changing from +5 to +4 under the pressure and temperature conditions for the synthesis. This type of valence change for an ion at high pressures and high temperatures was also found in the synthesis of $PbCrO_3$ perovskite [22]. The examined sample was then transferred to another DAC in which a liquid methanol–ethanol–water mixture at a volume ratio of 16:3:1 was used as a pressure medium to sustain a hydrostatic environment [23].

In situ high-pressure ADXRD experiments were performed at the 4W2 beam line of the Beijing Synchrotron Radiation Facility (BSRF). An image plate detector (MAR-345, the diameter of image is 345 mm) was used to collect diffraction patterns. The wavelength of the monochromatic x-ray beam was calibrated to be 0.6199 Å by scanning through the Mo metal K-absorption edge. The distance between the sample and the detector was calibrated to be 349.76 mm using CeO_2 as a standard. ADXRD patterns were collected with increasing pressure up to 10.6 GPa and also several patterns were collected in the decompression process. The collected diffraction patterns were analyzed by integrating images as a function of 2θ using the program Fit2D to obtain a conventional, one-dimensional diffraction profile [24]. Rietveld refinements of the 0.1 MPa and 6.4 GPa patterns were performed using GSAS software [25].

2.2. Calculation details

First-principles calculations were performed using the CASTEP code [26] based on density functional theory (DFT) with Vanderbilt-type ultrasoft pseudopotentials [27] and a plane-wave expansion of the wavefunctions. An energy cutoff of 750 eV was used for all calculations.

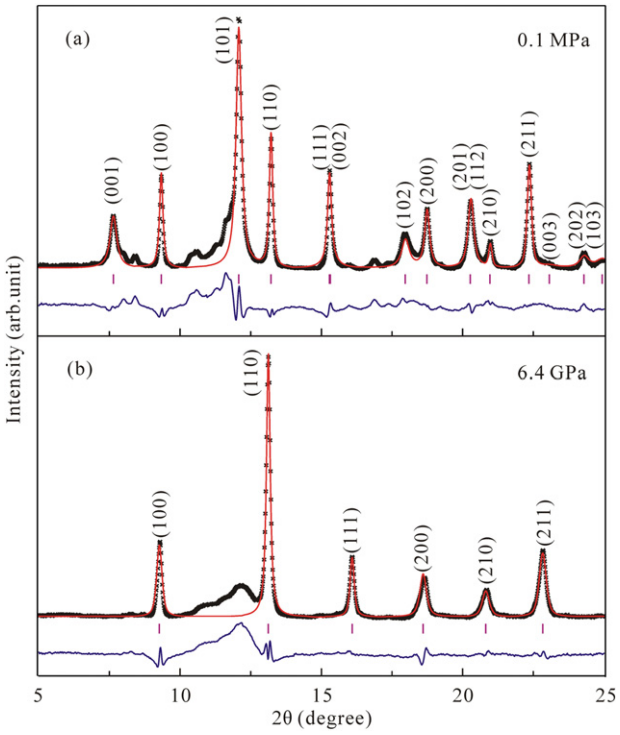

Figure 2. Observed and Rietveld refined powder ADXRD patterns of $PbVO_3$ perovskite at room temperature. (a) Tetragonal phase at ambient pressure (0.1 MPa) ($a = 3.8091(4)$ Å, $c = 4.6508(13)$ Å, fitting residuals; $R_p = 2.3\%$, $R_{wp} = 3.5\%$, and $\chi^2 = 0.75$). (b) Cubic phase at 6.4 GPa ($a = 3.8361(4)$ Å, fitting residuals; $R_p = 3.2\%$, $R_{wp} = 6.1\%$, and $\chi^2 = 0.77$). The observed and calculated patterns are shown as black crosses and red solid lines respectively. Small vertical ticks mark the calculated peak positions of the tetragonal and cubic phases. The blue solid curves show the difference between the observed and calculated patterns.

The exchange–correlation potential was treated within the local density approximation (LDA) [28] and the generalized gradient approximation (GGA) in the of PW91 [29], PBE [30] and WC schemes [31]. Pseudo-atomic calculations were performed for $Pb5d^{10}6s^26p^2$, $V3s^23p^63d^34s^2$ and $O2s^22p^4$. The numerical integration of the Brillouin zone was performed using a 0.03 Å^{-1} intervals Monkhorst–Pack *k*-point sample [32]. The self-convergence thresholds for energy change, maximum force, maximum stress, and maximum displacement between optimization cycles were 5×10^{-6} eV/atom, 0.01 eV Å^{-1}, 0.02 GPa and 5×10^{-4} Å, respectively. In the process, the optimized lattice parameters and energy values are obtained at various pressures.

3. Results

3.1. Experimental results

The ADXRD patterns of the sample collected at 0.1 MPa and 6.4 GPa, superimposed on the refinement results, are shown in figure 2. Most of the main diffraction lines for the 0.1 MPa pattern can be indexed into a tetragonal structure with $a = 3.8091(4)$ Å, $c = 4.6508(13)$ Å, and $V = 67.48(2)$ Å^3. The

Table 1. The atomic fractional coordinates and interatomic bond distances (Å) of the $PbVO_3$ *T*-phase obtained by the Rietveld refinement of our ADXRD experimental data at ambient pressure. Data within the square brackets corresponds to the results from first-principles calculations at zero pressure.

Atoms	*x*	*y*	*z*
Pb	0	0	0
V	0.5	0.5	0.5726(35) [0.5554]
O1	0.5	0.5	0.2157(35) [0.1985]
O2	0.5	0	0.6917(35) [0.6745]
Pb–O1 × 4	2.8742(3) [2.845]	V–O1 × 1	2.9909(5) [2.998]
Pb–O2 × 4	2.3840(3) [2.434]	V–O2 × 4	1.9835(2) [1.981]
		V–O1 × 1	1.6599(5) [1.664]

fitted lattice constants are in good agreement with previously presented values for the $PbVO_3$ *T*-phase [6, 7]. Several other weak peaks are attributed to unknown impurities produced by the complex sample synthesis process. The appearance of impurities has also occurred in bulk $PbVO_3$ sample synthesized by other HP-HT techniques [6, 7]. Both the (001) and (101) reflections, which are related to the *c*-axis of the $PbVO_3$ *T*-phase, show much broader full-width half-maxima (FWHM) than those of the (100) and (110) reflections, which are related only to the *a*-axis of the *T*-phase. This type of axis-dependent peak profile was also observed in previous work, where it was attributed to a strain effect induced by the unique layered structure of the $PbVO_3$ *T*-phase with large distortion [6]. The $PbVO_3$ *T*-phase (*P*4*mm*) was then modeled with the initial atomic positions taken from [7], where the Rietveld refinement of the 0.1 MPa pattern was performed. The structural refinement shows excellent residual values of $R_{wp} = 3.5\%$, $R_p = 2.3\%$ and reduced $\chi^2 = 0.75$. Table 1 shows that the refinement atomic positions and selected bond distances are similar to those of previous results [7]. The 6.4 GPa pattern shows six strong reflection peaks that can be perfectly indexed into a simple cubic structure with $a = 3.8361(4)$ Å and $V = 56.45(1)$ Å^3. The sharp and symmetric peaks indicate that there is no structural distortion in the XRD resolution of the cubic phase. The cell volume indicates that there is only one molecule of $PbVO_3$ in each unit cell, so the single cubic phase that was transformed from the $PbVO_3$ *T*-phase is concluded to be the cubic perovskite structure ($Pm\bar{3}m$). The structural refinement of the 6.4 GPa pattern, as shown in figure 2(b), with the residual values $R_p = 3.2\%$, $R_{wp} = 6.1\%$, and reduced $\chi^2 = 0.77$, also supports this conclusion.

Figure 3 shows several ADXRD patterns collected at different pressures and room temperature, indicating the reversible phase transition between the *T*-phase and *C*-phase of the $PbVO_3$ perovskites. New diffraction peaks, indexed

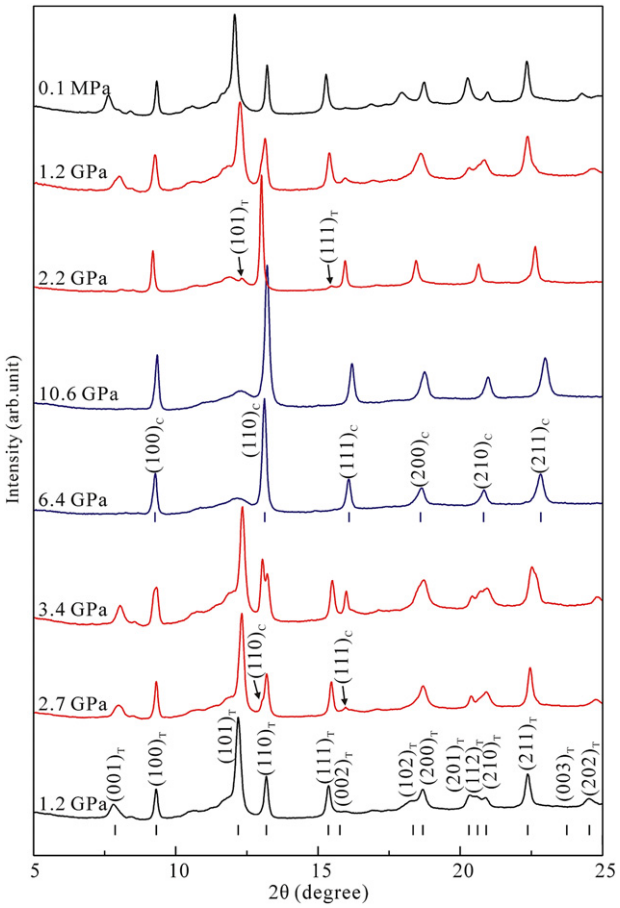

Figure 3. ADXRD patterns of $PbVO_3$ collected at various pressures during compression (lower patterns at pressures from 1.2 to 10.6 GPa) and decompression (upper patterns at 2.2 GPa, 1.2 GPa and 0.1 MPa) processes. Small vertical ticks just below the 0.7 GPa and the 6.4 GPa patterns are the calculated peak positions for Bragg reflections of the *P*4*mm* and $Pm\bar{3}m$ perovskites, respectively. The subscripts *T* and *C* denote the tetragonal phase and the cubic phase, respectively.

as the (110) and (111) lines of the *C*-phase, appeared when the pressure was increased to approximately 2.7 GPa. These peaks indicate the start of the structural transition from the *T*-phase to the *C*-phase of the $PbVO_3$ perovskites. The (110) peak of the *C*-phase is located at the low-angle position related to the (110) line of the *T*-phase, suggesting that the *a*-axis of the *C*-phase expands in contrast to the topologically relational *a*-axis of the *T*-phase. The intensity of the diffraction peaks of the *C*-phase increases gradually at the expense of the original diffraction peaks from the *T*-phase in the compression process until finally the diffraction peaks of the *T*-phase disappear completely at 6.4 GPa. The broad pressure range of *T*-phase and *C*-phase coexistence, which is very similar to previous observations [7], suggests that the phase transition is sluggish and therefore first order. No further structural transitions were observed up to the highest experimental pressure of 10.6 GPa in this study. Upon decompression, the inverse transformation from the *C*-phase to the *T*-phase is observed with some hysteresis. The transformation occurred at approximately 2.2 GPa, as evidenced by the appearance of

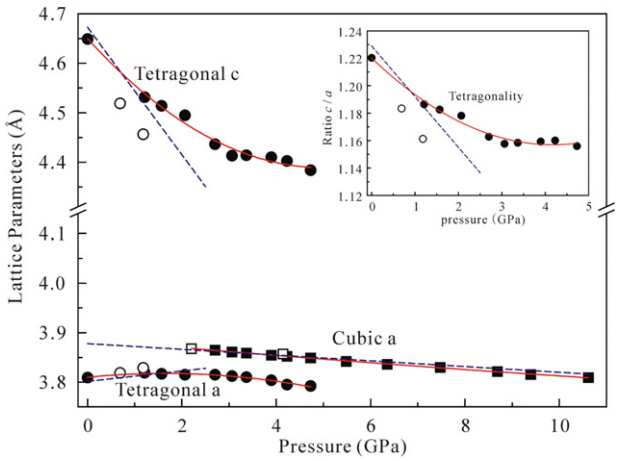

Figure 4. Pressure dependence of the lattice parameters of the $PbVO_3$ *T*-phase and *C*-phase and the tetragonality of the *T*-phase (see inset) at room temperature. Solid symbols (circles and squares) represent experimental data obtained during the compression process and open symbols represent decompression experimental data. The blue dashed lines represent first-principles calculated results. The red solid lines represent fitting results for observed *a* and *c* values as well as tetragonality using a quadratic polynomial function (decompression data at 0.7 and 1.2 GPa are not included in the fitting).

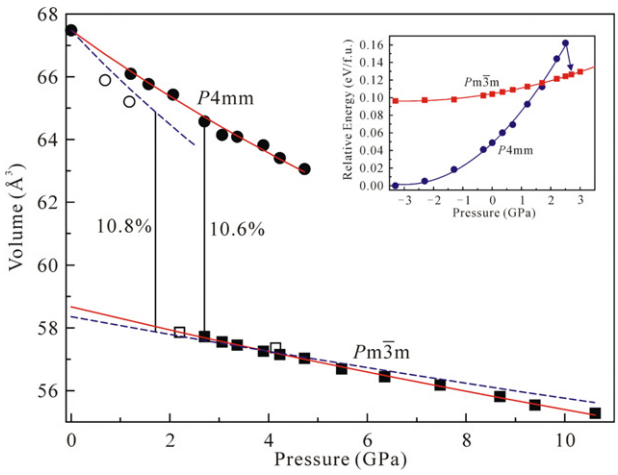

Figure 5. Experimental and theoretical pressure–volume data as well as the total energy (see inset) of the $PbVO_3$ *T*-phase and *C*-phase. Solid and open symbols (circles and squares) represent the experimental data obtained in the compression and decompression processes, respectively. The red solid curves represent fitting results of experimental data using the Birch–Murnaghan equation of state and the blue dashed curves are the results of first-principles calculations. The vertical lines are guides for the eye.

the (101) and (111) diffraction peaks of the *T*-phase, and was complete at atmospheric pressure.

The pressure dependence of the lattice parameters of the *T*-phase and *C*-phase and the tetragonality of the *T*-phase (inset) at room temperature are plotted in figure 4. The lattice parameters of the *C*-phase can be fitted approximately by a linear function of pressure (shown as a solid red line): a (Å) $= 3.8828(9) - 0.0071(2) \times P$ (GPa) with a coefficient of determination of $R^2 = 0.994$, even though the normal compression behavior should be non-linear. It decreases by 1.4% as pressure increases from 2.7 to 10.6 GPa. However, the lattice parameters of the *T*-phase show an irregular dependence on pressure: the parameters were fitted using quadratic polynomial functions and plotted as solid red curves to guide the eye. The *T*-phase *a* constant increased slightly as the pressure increased up to 2.7 GPa and then decreased over the pressure range of *T*-phase and *C*-phase coexistence, i.e. from 2.7 to 4.7 GPa. The *c* constant of the *T*-phase decreases as much as 4.6% from atmospheric pressure to 2.7 GPa and then further decreases by only 1.2% from 2.7 to 4.7 GPa. It is noteworthy that the change of the *c* constant with pressure is much greater than that of the *a* constant; therefore, the $PbVO_3$ *T*-phase exhibits a remarkable level of anisotropic compressibility. The irregular behavior of the *a* and *c* constants of the *T*-phase with changing pressure results in an abnormal change of tetragonality of the *T*-phase with increasing pressure, decreasing quickly from zero pressure to 2.7 GPa and then decreasing slowly from 2.7 to 4.7 GPa. In addition, the *P*–*c* data for the *T*-phase in figure 4 shows that the *c* constants at 0.7 and 1.2 GPa clearly deviate from the total *P*–*c* trend in showing much smaller values. At the same time, the corresponding *a* constants follow the *P*-*a* trend. The 0.7 and 1.2 GPa diffraction data were collected during the decompression process, when the *T*-phase was transformed from the *C*-phase. This type of phenomenon is induced by the existing strain along the *c*-axis owing to the layered structure of the *T*-phase. For this reason, the two data points are omitted for all of the data analysis although they are still shown in the diagrams.

The experimental pressure–volume data for both the *T*-phase and *C*-phase are plotted in figure 5. A large volume difference of 10.6% between the *T*-phase and the *C*-phase was observed in the two-phase coexistence region at 2.7 GPa. Although the *a* and *c* constants exhibit irregular compressed features, the unit cell volumes of the *T*-phase do not show an abnormal trend with increasing pressure. Fitting the two sets of *P*–*V* data for both the *T*-phase and the *C*-phase with the Birch–Murnaghan equation of state (EOS), using a fixed bulk modulus pressure derivative (K_0') of 4, yields a bulk modulus $K_0 = 61(2)$ GPa and a unit cell volume $V_0 = 67.4(1)$ Å^3 for the *T*-phase and values of $K_0 = 155(3)$ GPa and $V_0 = 58.67(4)$ Å^3 for the *C*-phase. The $PbVO_3$ *T*-phase exhibits a much larger compressibility than the $PbVO_3$ *C*-phase.

3.2. Calculation results

The total energy calculations using various exchange–correlation functionals predict that the C-AFM and nonmagnetic states are the ground states of the $PbVO_3$ tetragonal and cubic perovskites, respectively. These results are in good agreement with previous studies [19], where the detailed electronic properties of the ground states of both phases were also given. In this paper, the first-principles calculations mainly focused on the structural behavior of the $PbVO_3$ perovskites at high pressures to describe our experimental observations. Although the lattice parameters and interatomic

distances calculated within the GGA-WC scheme are in good agreement with the experimental results, the total energy of the cubic phase is 0.22 eV lower than that of the tetragonal phase, suggesting the C-AFM *T*-phase is less stable than the NM *C*-phase at zero pressure, which is opposite to the experimental results. On the other hand, the total energy of the unit C-AFM *T*-phase calculated within the GGA-PBE scheme is approximately 0.1 eV lower than that of the NM *C*-phase at zero pressure. This calculation correctly describes the experimental findings, so the following calculations were performed using the GGA-PBE method for the C-AFM *T*-phase and NM *C*-phase of the $PbVO_3$ perovskites.

The calculated unit cell volume of the $PbVO_3$ tetragonal perovksite at zero pressure is approximately 7% larger than the corresponding experimental value. When a pressure of 3.3 GPa is applied the calculated volume is in excellent agreement with the experimental volume of the *T*-phase at atmosphere pressure. To describe the experimental results well, a pressure correction of 3.3 GPa is subsequently employed to correct the calculated results. This type of pressure correction has also been applied in some other calculations [33, 34]. The calculated lattice parameters at corrected zero pressure are $a = 3.8091$ Å and $c = 4.6614$ Å, which are also in good accordance with the experimental values. The calculated atomic fractional coordinates and atomic distances at zero pressure are listed in table 1.

The inset in figure 5 shows the energies of both the *T*-phase and the *C*-phase at different pressures. The energy of the *T*-phase exceeds that of the *C*-phase at approximately 1.7 GPa, indicating that the phase transition from the *T*-phase to the *C*-phase occurs at that pressure. The calculated transition pressure is close to the experimental observation of 2.7 GPa. The C-AFM *T*-phase calculation can be performed to a pressure of 2.5 GPa; however, as denoted by the arrow symbol, the C-AFM *T*-phase collapses to the NM *C*-phase when a pressure of 2.7 GPa is applied. This type of phase collapse was also predicted by previous calculations [19].

The theoretical pressure dependence of the lattice parameters of both the *T*-phase and the *C*-phase and the tetragonality of the *T*-phase are plotted as dashed blue lines in figure 4. The *c* constant decreases rapidly with increasing pressure. However, the *a* constant increases with a smaller magnitude in comparison with the *c* constant, resulting in a rapid decrease of the tetragonality with pressure. The predicted dependence of the *a* and *c* constants of the *T*-phase with pressure (and thus the c/a ratio) agree with experimental observations in the range of zero pressure to 2.7 GPa; however, at pressures above 2.7 GPa, there exist obvious deviations between the theoretical and experimental results, especially the experimental *a* constants become decreasing with pressure. We suggest that the experimentally observed abnormal changes of the *a* and *c* constants with pressure in the 2.7–4.7 GPa range, as described above, are produced by the coexistence of the *T*-phase and the *C*-phase during the transition process. However, the anomaly in the pressure dependence of the *a* constant of the *T*-phase might be essential, as the very same anomaly was also observed in $PbTiO_3$ perovskite [34, 35]. The calculated lattice constants

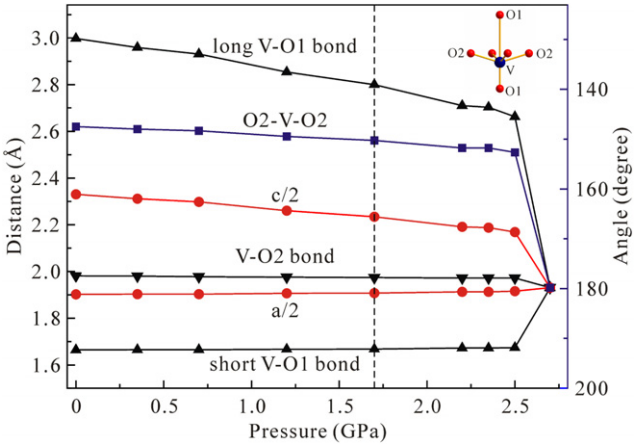

Figure 6. Various V–O bond lengths, the O2–V–O2 angle and *a* and *c* lattice parameters (displayed here as $a/2$ and $c/2$) of the $PbVO_3$ *T*-phase as a function of pressure. The data are obtained from first-principles calculations.

of the *C*-phase at different pressures are in perfect agreement with the experimental results. The theoretical lattice constant of 3.8790 Å at zero pressure is very close to that of the experimentally extrapolated value of 3.8857 Å.

The theoretical *P*–*V* data of both the *T*-phase and the *C*-phase are plotted as dashed blue lines in figure 5. A large volume collapse of 10.8% is predicted at the phase transition between the *T*-phase and the *C*-phase at 1.7 GPa. The calculated volume collapse is in excellent agreement with the corresponding experimental observation of 10.6% at 2.7 GPa. Fitting the two sets of theoretical *P*–*V* data for both the *T*-phase and the *C*-phase with the Birch–Murnaghan equation of state (EOS) with a fixed K_0' of 4 yields a bulk modulus $K_0 = 38(1)$ GPa and a unit cell volume $V_0 = 67.65(9)$ Å^3 for the *T*-phase, and values of $K_0 = 200.2(3)$ GPa and $V_0 = 58.361(3)$ Å^3 for the *C*-phase. The theoretical K_0 value of the *T*-phase is smaller than the experimental value, which frequently occurs with the GGA scheme. On the other hand, the theoretical value of K_0 of the *C*-phase is larger than the experimental observed value.

The predicted pressure dependence of the various V–O bond lengths, the O2–V–O2 angle, and the *a* and *c* constants (displayed as $a/2$ and $c/2$, respectively) of the *T*-phase are plotted in figure 6. The corresponding parameters of the NM *C*-phase, collapsed from the C-AFM *T*-phase at 2.7 GPa, are also displayed. The length of the long V–O1 bond decreases rapidly for pressure increases up to 2.5 GPa; however, the increase in the length of the short V–O1 bond is much smaller in magnitude, and the *c* constant decreases considerably as a result. At the same time, although the V–O2 bond shortens slightly, the increment of the O2–V–O2 angle makes the *a* constant increase slightly. Therefore, the rapid contraction in volume of the *T*-phase with pressure is due to the rapid shortening of the long V–O1 bond. Figure 1(a) shows that from an atomic point of view, all of the above-mentioned changes are induced by the VO_5 coordinated pyramidal shifting totally along the *c*-axis with the O1 to close the Pb atomic plane with increasing pressure. This demonstrates the

weak interaction between the VO_5 pyramidal layers in the large distorted tetragonal structure. For all that, the *T*-phase still remains a large tetragonal distortion feature even at 2.5 GPa, with a c/a ratio of 1.132. When the structure of the *T*-phase collapses at 2.7 GPa, the values of all of the parameters mentioned above change abruptly to values for the *C*-phase with an ideal VO_6 coordinated octahedron, as shown in figure 1(b), indicating that the electronic interaction of both the long and the short V–O bonds changes distinctly. Although the theoretical transition pressure is predicted to be 1.7 GPa by the energy intersection between the *T*-phase and the *C*-phase, the structural collapse of the *T*-phase also illustrates the atomic picture of the electronic phase transition very well.

4. Discussion

The tetragonal phase of $PbVO_3$ perovskite possesses a tetragonally distorted perovskite structure with an elongated direction along the *c*-axis. Both our synchrotron powder ADXRD experiments and first-principles calculations for the $PbVO_3$ system reveal that the *T*-phase is a thermodynamically stable phase at ambient condition. In a unit cell, the central V atom is coordinated with five O atoms which are arranged in a VO_5 square pyramid configuration with the apex O atom (O1) at the *c*-axis of the tetragonal cell and four base vertex O atoms (O2) on the lateral faces (see figure 1). The short V–O1 bond has a bond length of 1.6599 Å, which is much smaller than the V–O2 bond length (1.9835 Å). The vanadyl bond defined by Clark [35] posits the short V–O1 bond as a V=O double bond, with a π-component arising from the electron flow from the O($p\pi$) to the V(dπ) orbitals [36]. The existence of the V=O double bond parallel to the *c*-axis is most likely the determining factor for the tetragonal distortion of the *T*-phase. Each of the four base vertex O atoms of the VO_5 square pyramid is shared with a neighboring square pyramid in the lattice, forming a layer structure of VO_5 square pyramids that are perpendicular to the *c*-axis. As indicated by the large difference between the long V–O1 bond length and the V–O2 bond length, the intra-layer binding force is strong, while the inter-layer force is weak. The weak inter-layer force in the *c*-direction is also reflected in the width of diffraction peaks [37]; for example, the (001) peak associated with the *c*-axis shows a much broader FWHM than the (100) peak that is associated with the *a*-axis. The characteristics of the crystal structure, especially the layered structure of the *T*-phase, results in a high compressional anisotropy, with the soft direction being along the *c*-axis, as shown in figure 4. This anisotropic compressibility is also common in other vanadates with a V=O vanadyl bond. For example, in NaV_2O_5, the *c* parameter decreases by 24% at 29 GPa, whereas the *a* and *b* parameters show a much smaller change of 1% [38].

Table 2 lists the bulk moduli of several compounds with a perovskite structure. We found that the bulk modulus of the $PbVO_3$ *T*-phase is comparable to that of the $BiCoO_3$ *T*-phase [18] but much smaller than that of $PbTiO_3$ [39] and $BaTiO_3$ [17]. These differences in the bulk moduli can be interpreted in terms of the degree of tetragonal distortion. The distortion of the $PbVO_3$ *T*-phase ($c/a = 1.22$) is similar to that of the $BiCoO_3$ ($c/a = 1.27$) *T*-phase but much larger than that of the $PbTiO_3$ *T*-phase ($c/a = 1.06$) and the $BaTiO_3$ *T*-phase ($c/a = 1.01$). Note that the *T*-phase for each material exhibits a much lower value of bulk modulus than for the *C*-Phase: the *T*-phase bulk moduli are lower than 104 GPa except for $PbTiO_3$, while the *C*-phase bulk moduli range from 141 to 195 GPa. The $PbVO_3$ *C*-phase possesses a bulk modulus comparable to the $SrVO_3$ *C*-phase [40], the $PbTiO_3$ *C*-phase, and the $PbCrO_3$ cubic phase II [22].

Table 2. The bulk moduli of the $PbVO_3$ *T*-phase and *C*-phase and several related compounds with tetragonal and cubic perovskite structures.

	Structure	K_0 (GPa)	K_0'	Reference
$PbVO_3$	Tetragonal	61(2)	4	This work
	Cubic	155(3)	4	
$SrVO_3$	Cubic	147	—	[40]
$PbTiO_3$	Tetragonal	100(3)	4	[15]
		104(4)		[39]
	Cubic	195(3)	4	[15]
		141(5)		[39]
$BaTiO_3$	Tetragonal	135	6.4	[17]
		179(3)	4	[42]
$BiCoO_3$	Tetragonal	74(3)	4	[18]
	Orthorhombic	104(3)	4	
$PbCrO_3$	Cubic phase I	59(5)	4	[22]
	Cubic phase II	187(4)		

The phase transition from tetragonal to cubic perovskite in $PbVO_3$ mainly involves the displacement of atoms in the *c*-direction, showing no distinct change in atomic packing (see figure 1). Therefore, the phase transition can be taken as a displacive phase transition that occurs in typical ferroelectric perovskite materials such as $PbTiO_3$ and $BaTiO_3$ [15, 17]. However, unlike typical displacive phase transitions, the *T*-to-*C* transition in $PbVO_3$ perovskites is a sluggish process with a broad pressure range for two-phase coexistence (2.7–6.4 GPa), which is probably intrinsic to the phase transition as a hydrostatic pressure medium was used in the present work. The observed broad pressure range for two-phase coexistence might imply that a potential energy barrier exists between the *T*-phase and the *C*-phase. During the *T*-to-*C* phase transition, the π-component of the short V–O1 bond (V=O vanadyl bond) breaks down to form a V–O single bond which is similar to the V–O2 equatorial bond. The change of the V=O vanadyl bond to a V–O single bond requires a large activation energy to overcome the energy barrier. In the phase transition process, the coordination polyhedron of O atoms around the central V atom changes from a polar square pyramid in the *T*-phase to an isotropic octahedron in the *C*-phase. In the case of pyramidal coordination, the d-orbitals of the central V atom split into b_{2g} (d_{xy}), doubly degenerate e_g (d_{xz} and d_{yz}), a_{1g} (d_{z^2}), and b_{1g} ($d_{x^2-y^2}$) energy levels, while for octahedral coordination, the d-orbitals split into triply degenerate t_{2g} (d_{xy}, d_{xz}, d_{yz}) and doubly degenerate e_g (d_{z^2} and $d_{x^2-y^2}$) energy levels [19]. Hence, the *T*-to-*C* transition for $PbVO_3$ is accompanied by a distinct change in the electronic structure of the V^{4+} ion.

This change in electronic structure has been demonstrated by resistivity measurements which revealed an insulator–metal transition for $PbVO_3$ perovskite across the *T*-to-*C* phase transition [7]. Here, we predict that the large volume collapse of 10.6% for the *T*-to-*C* transition of $PbVO_3$ occurs mainly due to a transition in the electronic structure. A large volume change is also observed for the phase transition of $BiCoO_3$ perovskite with a change in the electronic structure [18].

$PbVO_3$ tetragonal perovskite is a candidate multiferroic as it shows two-dimensional antiferromagnetism with long-range order at T_N = 43–50 K [10] and a large spontaneous polarization of 152 μC cm^{-2} [9]. However, polarization–electric-field (P–E) hysteresis has not been observed in the bulk $PbVO_3$ *T*-phase even under an electric field of 90 kV cm^{-1} at liquid nitrogen temperature [7]. An effective piezoelectric coefficient d_{33} of about 3.1 pC N^{-1} was obtained for $PbVO_3$ thin films [41], which indicates that $PbVO_3$ is polar and piezoelectric and therefore likely to be ferroelectric. The large tetragonal distortion and the formation of a VO_5 square pyramidal structure with a short V=O vanadyl bond may limit the ferroelectric switchability of the $PbVO_3$ *T*-phase. The ferroelectric transition of the $PbVO_3$ *T*-phase has not yet been observed, even up to the oxidation temperature of 570 K at ambient pressure [7]; however, the transition can be realized at high pressure. Applying chemical pressure by atom substitution may reduce the pressure of the phase boundary to ambient pressure. For example, high electromechanical coupling in $PbTiO_3$–$PbZrO_3$ and $PbMg_{1/3}Nb_{2/3}O_3$–$PbTiO_3$ solid solutions results from B-site substitution in $PbTiO_3$, which tunes the morphotropic phase boundary from high pressure to ambient pressure [13]. The ferroelectric transition in $PbVO_3$ perovksite exhibits a broad pressure range for the two coexisting phases and is reversible. Atom substitution and doping of the A-sites or B-sites in $PbVO_3$ perovskite may tune the coexisting phase region to lower pressures or even to ambient pressure. The ferroelectric transition can then easily occur by applying an electric field and the polarization of the tetragonal phase can be switched across the *T*-to-*C* phase boundary. Atom substitution and doping of the A-sites and B-sites in $PbVO_3$ perovskite may help us develop new high-performance electromechanical compounds.

5. Conclusions

High-pressure synchrotron ADXRD experiments under hydrostatic conditions up to 10.6 GPa at room temperature and first-principles theoretical calculations were carried out to investigate the structural properties of $PbVO_3$ perovskite under compression. We found that the compression behavior of the $PbVO_3$ *T*-phase is highly anisotropic with the *c*-axis being the soft direction, and a reversible *T*-to-*C* (tetragonal to cubic) perovskite structural phase transition was found to occur between 2.7 and 6.4 GPa in the compression process and below 2.2 GPa in the decompression process. The *T*-phase possesses a large tetragonal distortion that may be mainly determined by the V=O double bond (short V–O1 bond) in the pyramidal coordination polyhedron of O atoms around the central V atom, which is parallel to the *c*-axis. The *T*-to-*C* transition is similar to a displacive phase transition but shows a distinct change in electronic structure. The polar pyramidal coordination of the V^{4+} ion in the *T*-phase changes to an isotropic octahedral coordination in the *C*-phase, and the V=O double bond breaks down to form a V–O single bond in the *C*-phase. A large volume collapse of 10.6% was observed at 2.7 GPa for the *T*-to-*C* transition, which was interpreted to originate mainly from the electronic structural change of the V^{4+} ion. Fitting the observed *P*–*V* data using the Birch–Murnaghan equation of state with a fixed value of K_0' of 4, yields a bulk modulus K_0 = 61(2) GPa and volume V_0 = 67.4(1) Å^3 for the *T*-phase and values of K_0 = 155(3) GPa and V_0 = 58.67(4) Å^3 for the *C*-phase, respectively.

Acknowledgments

We gratefully acknowledge the assistance from High Pressure Beam Line, BSRF, China. This work has been supported by the National Natural Science Foundation of China (41090373, 11179030, 41174072, 41272058, 41121002, 40772029) and the Knowledge Innovation Project of the Chinese Academy of Sciences (KJCX2-SW-N20, KJCX2-YW-Q08-03-4). This is contribution No. IS-1559 from GIGCAS.

References

[1] Hill N A 2000 *J. Phys. Chem.* B **104** 6694
[2] Spaldin N A and Fiebig M 2005 *Science* **309** 391
[3] Fiebig M 2005 *J. Phys. D: Appl. Phys.* **38** R123
[4] Hur N, Park S, Sharma P, Ahn J, Guha S and Cheong S 2004 *Nature* **429** 392
[5] Nan C W, Bichurin M, Dong S, Viehland D and Srinivasan G 2008 *J. Appl. Phys.* **103** 031101
[6] Shpanchenko R V, Chernaya V V, Tsirlin A A, Chizhov P S, Sklovsky D E, Antipov E V, Khlybov E P, Pomjakushin V, Balagurov A M and Medvedeva J E 2004 *Chem. Mater.* **16** 3267
[7] Belik A A, Azuma M, Saito T, Shimakawa Y and Takano M 2005 *Chem. Mater.* **17** 269
[8] Uratani Y, Shishidou T and Oguchi T 2009 *J. Phys. Soc. Japan* **78** 084709
[9] Uratani Y, Shishidou T, Ishii F and Oguchi T 2005 *Japan. J. Appl. Phys.* **44** 7130
[10] Oka K, Yamada I, Azuma M, Takeshita S, Satoh K H, Koda A, Kadono R, Takano M and Shimakawa Y 2008 *Inorg. Chem.* **47** 7355
[11] Wu Z and Cohen R E 2005 *Phys. Rev. Lett.* **95** 37601
[12] Sanjurjo J, Lopez-Cruz E and Burns G 1983 *Phys. Rev.* B **28** 7260
[13] Ahart M, Somayazulu M, Cohen R, Ganesh P, Dera P, Mao H, Hemley R J, Ren Y, Liermann P and Wu Z 2008 *Nature* **451** 545
[14] Glazer A and Mabud S 1978 *Acta Crystallogr.* B **34** 1065
[15] Sani A, Hanfland M and Levy D 2002 *J. Phys.: Condens. Matter* **14** 10601
[16] Venkateswaran U D, Naik V M and Naik R 1998 *Phys. Rev.* B **58** 14256
[17] Pruzan P, Gourdain D, Chervin J, Canny B, Couzinet B and Hanfland M 2002 *Solid State Commun.* **123** 21
[18] Oka K, Azuma M, Chen W, Yusa H, Belik A A, Takayama-Muromachi E, Mizumaki M, Ishimatsu N, Hiraoka N and Tsujimoto M 2010 *J. Am. Chem. Soc.* **132** 9438

[19] Ming X, Yin J-W, Wang X-L, Wang C-Z, Huang Z-F and Chen G 2010 *Solid State Sci.* **12** 938
[20] Shannon R D and Calvo C 1973 *Can. J. Chem.* **51** 70
[21] Mao H, Xu J and Bell P 1986 *J. Geophys. Res.* **91** 25
[22] Xiao W, Tan D, Xiong X, Liu J and Xu J 2010 *Proc. Natl Acad. Sci. USA* **107** 14026
[23] Klotz S, Chervin J, Munsch P and Le Marchand G 2009 *J. Phys. D: Appl. Phys.* **42** 075413
[24] Hammersley A, Svensson S, Hanfland M, Fitch A and Hausermann D 1996 *High Press. Res.* **14** 235
[25] Larson A C and Von Dreele R B 2004 General structure analysis system (GSAS) *Los Alamos National Laboratory Report LAUR 86*
[26] Clark S J, Segall M D, Pickard C J, Hasnip P J, Probert M I J, Refson K and Payne M C 2005 *Z. Kristallogr.* **220** 567
[27] Vanderbilt D 1990 *Phys. Rev.* B **41** 7892
[28] Ceperley D M and Alder B 1980 *Phys. Rev. Lett.* **45** 566
[29] Perdew J P, Chevary J, Vosko S, Jackson K A, Pederson M R, Singh D and Fiolhais C 1992 *Phys. Rev.* B **46** 6671
[30] Perdew J P, Burke K and Ernzerhof M 1996 *Phys. Rev. Lett.* **77** 3865
[31] Wu Z and Cohen R E 2006 *Phys. Rev.* B **73** 235116
[32] Monkhorst H J and Pack J D 1976 *Phys. Rev.* B **13** 5188
[33] Vanderbilt D 1998 *J. Korean Phys. Soc.* **32** S103
[34] Walker A M 2012 *Phys. Earth Planet. Inter.* **192/193** 81
[35] Clark R J H 1968 *The Chemistry of Titanium and Vanadium: An Introduction to the Chemistry of the Early Transition Elements* (Amsterdam: Elsevier)
[36] Ballhausen C J and Gray H B 1962 *Inorg. Chem.* **1** 111
[37] Loa I, Grzechnik A, Schwarz U, Syassen K, Hanfland M and Kremer R K 2001 *J. Alloys Compounds* **317/318** 103
[38] Loa I, Syassen K, Kremer R, Schwarz U and Hanfland M 1999 *Phys. Rev.* B **60** 6945
[39] Zhu J, Xu H, Zhang J, Jin C, Wang L and Zhao Y 2011 *J. Appl. Phys.* **110** 084103
[40] Maekawa T, Kurosaki K and Yamanaka S 2006 *J. Alloys Compounds* **426** 46
[41] Kumar A, Martin L W, Denev S, Kortright J B, Suzuki Y, Ramesh R and Gopalan V 2007 *Phys. Rev.* B **75** 060101
[42] Kumar R S, Cornelius A L and Nicol M F 2007 *Phys. Status Solidi* b **244** 290